

Supporting Information

A Highly Stretchable Nanofiber-based Electronic Skin with Pressure-, Strain-, and Flexion-sensitive Properties for Health and Motion Monitoring

**Kun Qi^a, Jianxin He^{b,c*}, Hongbo Wang^{a*}, Yuman Zhou^a, Xiaolu You^{b,c}, Nan Nan^{b,c}, Weili Shao^{b,c},
Lidan Wang^{b,c}, Bin Ding^{b,d}, Shizhong Cui^{b,c}**

^a School of Textile and Clothing, Jiangnan University, Wuxi 214122, China

^b Provincial Key Laboratory of Functional Textile Materials, Zhongyuan University of Technology, Zhengzhou 450007, China

^c Collaborative Innovation Center of Textile and Garment Industry, Zhengzhou 450007, China Henan

^d Key Laboratory of Textile Science & Technology, Ministry of Education, College of Textiles, Donghua University, Shanghai 201620, China

Corresponding author: Jianxin He

P.O. Box 110, College of Textiles, Zhongyuan University of Technology, 41 Zhongyuan Road, Zhengzhou City 450007, Henan Province, People's Republic of China

E-mail: hejianxin771117@163.com

Co-corresponding author: Hongbo Wang

School of Textile and Clothing, Jiangnan University, 1800 Lihu Road, Wuxi City 214122, Jiangsu Province, People's Republic of China

E-mail: wxwanghb@163.com

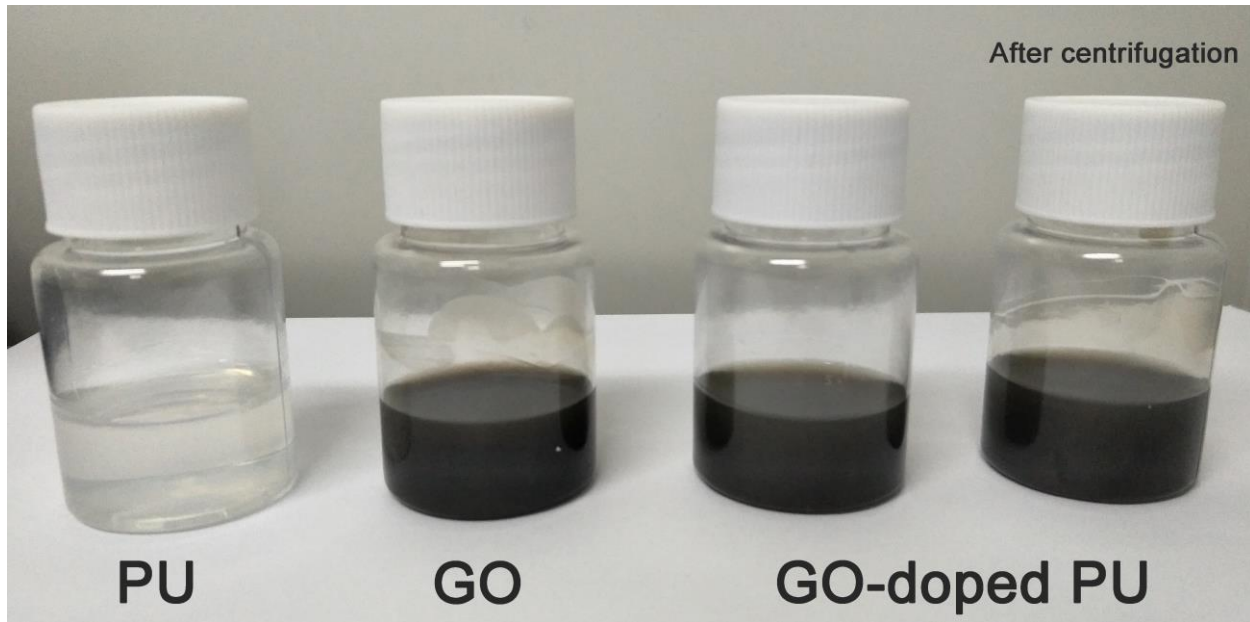
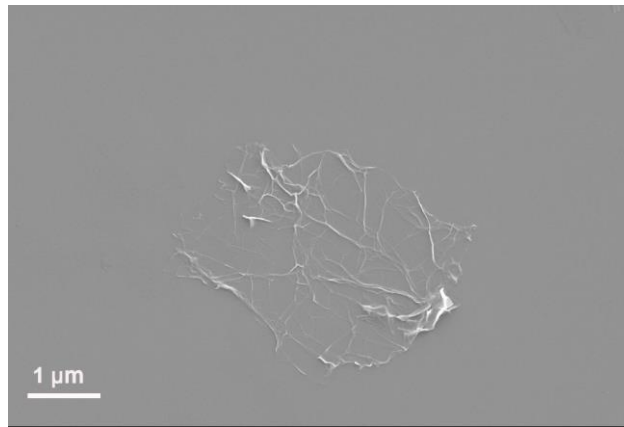
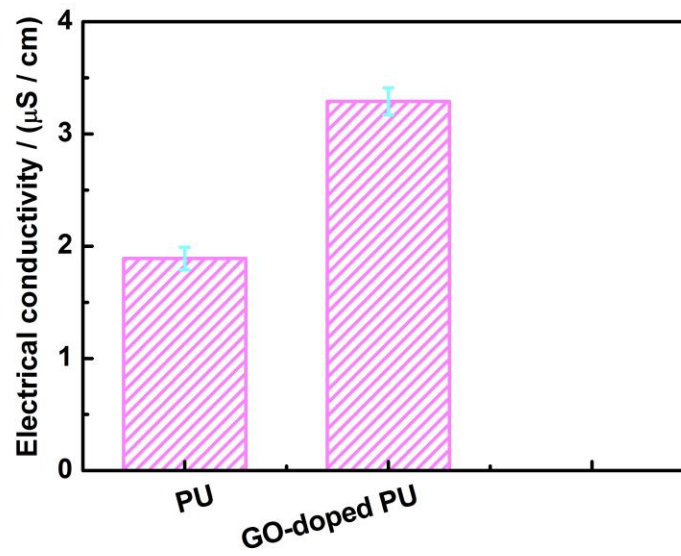


Fig.S1. Photograph of the well suspended PU electrospinning solution, GO dispersion solution, , GO-doped PU electrospinning solution before and after centrifugation, respectively



(a)



(b)

Fig.S2. (a) The SEM of the GO nanosheet. Ripples and wrinkles are observed in the micron-scale GO nanosheet. (b) The electrical conductivity of PU and GO-doped PU solution.

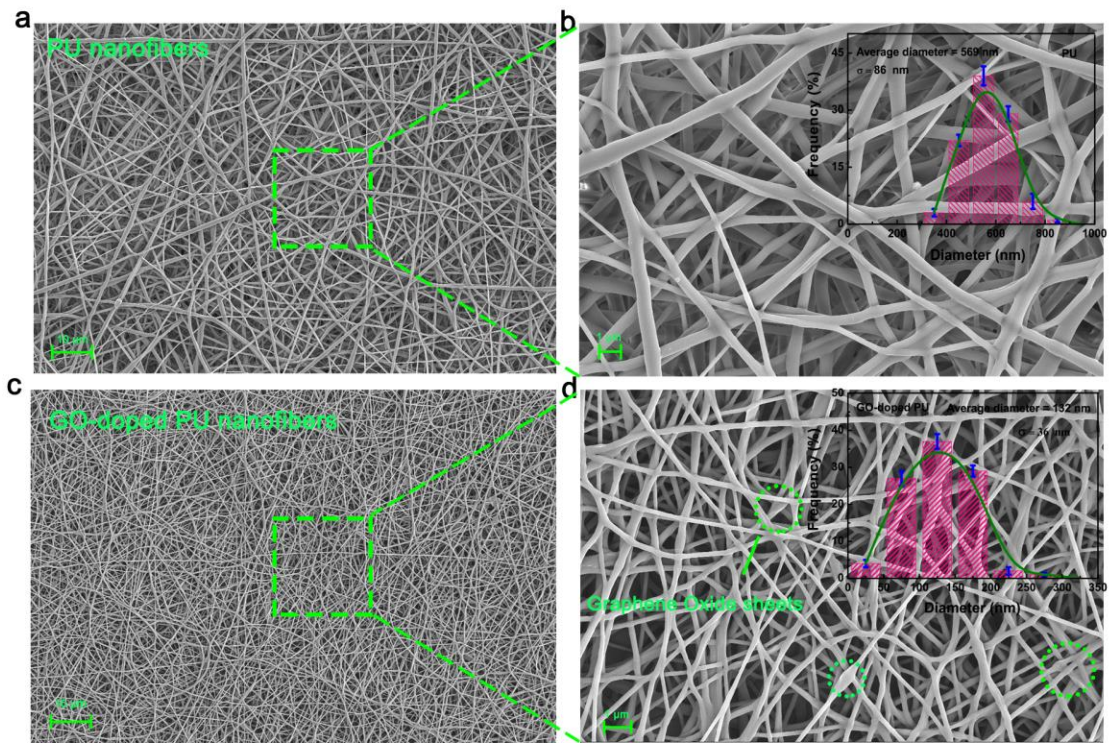


Fig. S3 The low and high magnification SEM micrographs and diameter distribution histograms of (a-b) pure PU, (c-d) GO-doped PU nanofibers.

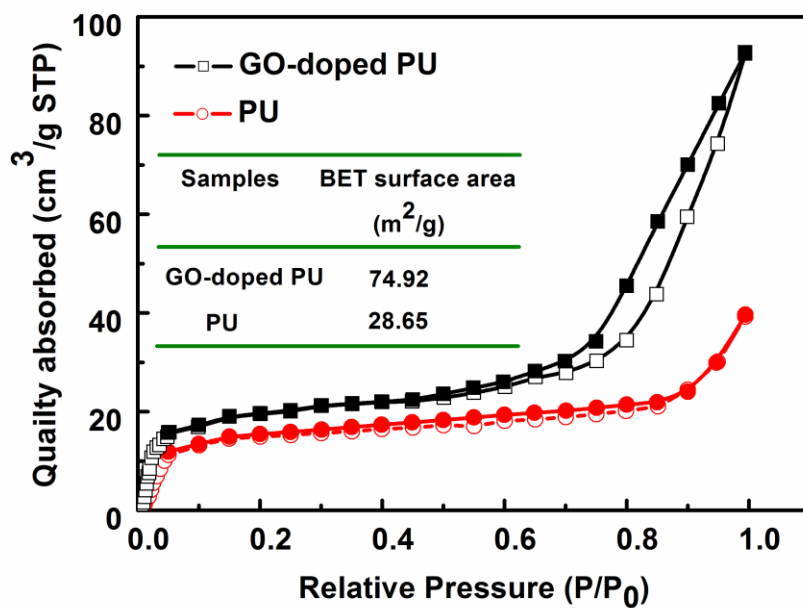


Fig. S4 N₂ adsorption–desorption isotherms curves of PU and GO-doped nanofibers. The inset table shows the BET surface area of PU and GO-doped nanofibers.

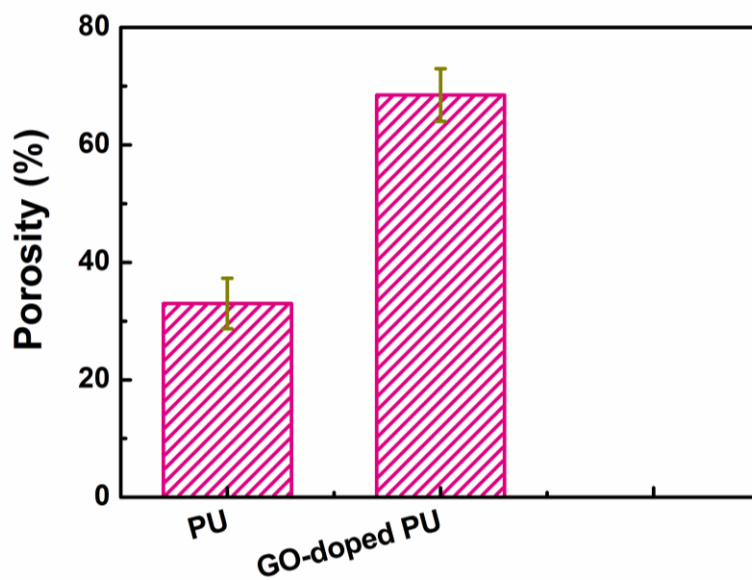


Fig. S5 The porosity of electrospun PU, and GO-doped PU nanofiber substrate.

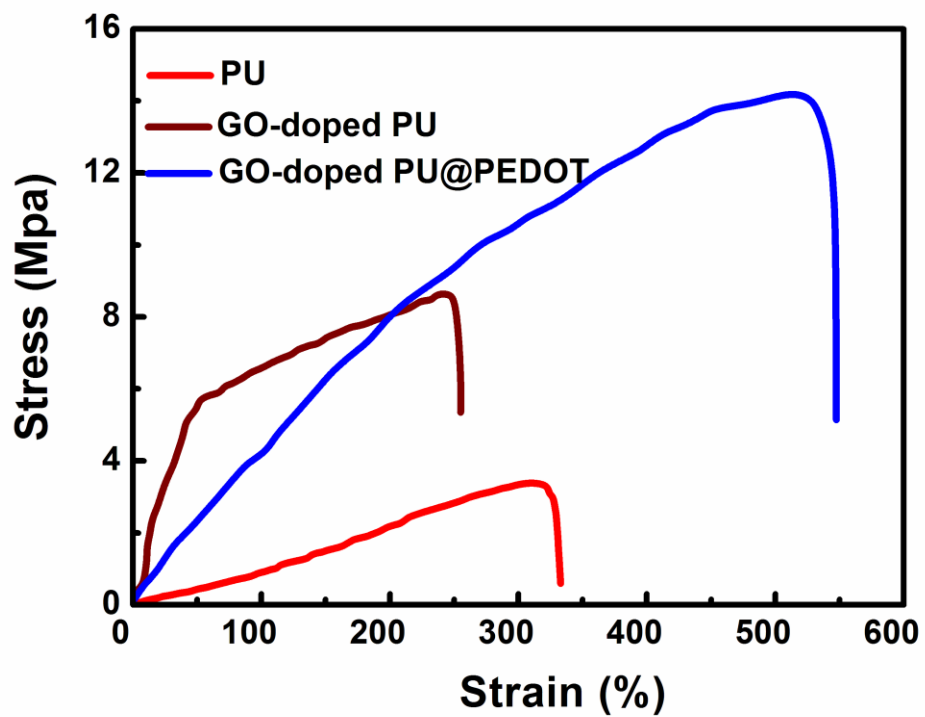


Fig.S6 Typical stress-strain curves of the pure electrospun fibrous PU, GO-doped PU, and GO-doped PU@PEDOT mats (n = 10 for all types of nanofibers), tested at room temperature.

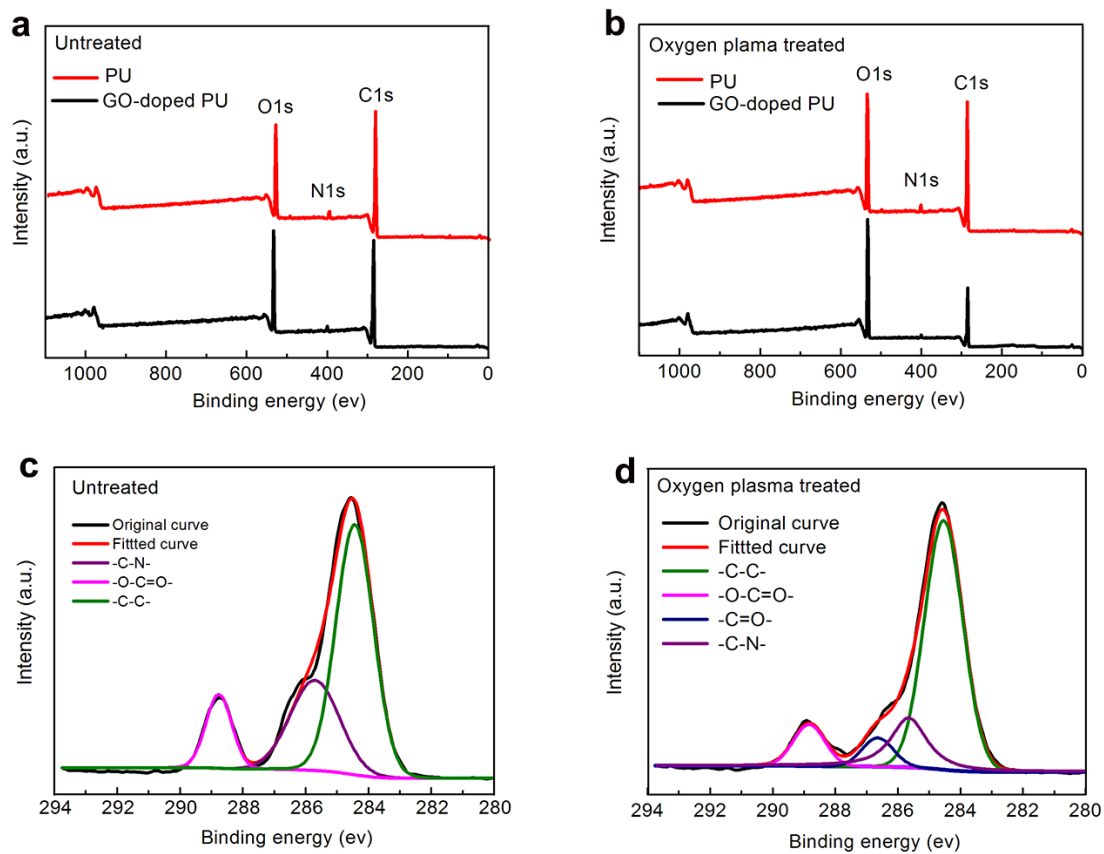


Fig. S7 XPS survey spectra of PU and GO-Doped PU nanofiber membrane before (a) and after (b) low-temperature oxygen plasma treatment; C1s XPS spectra of GO-Doped PU nanofiber membrane before (c) and after (d) low-temperature oxygen plasma treatment.

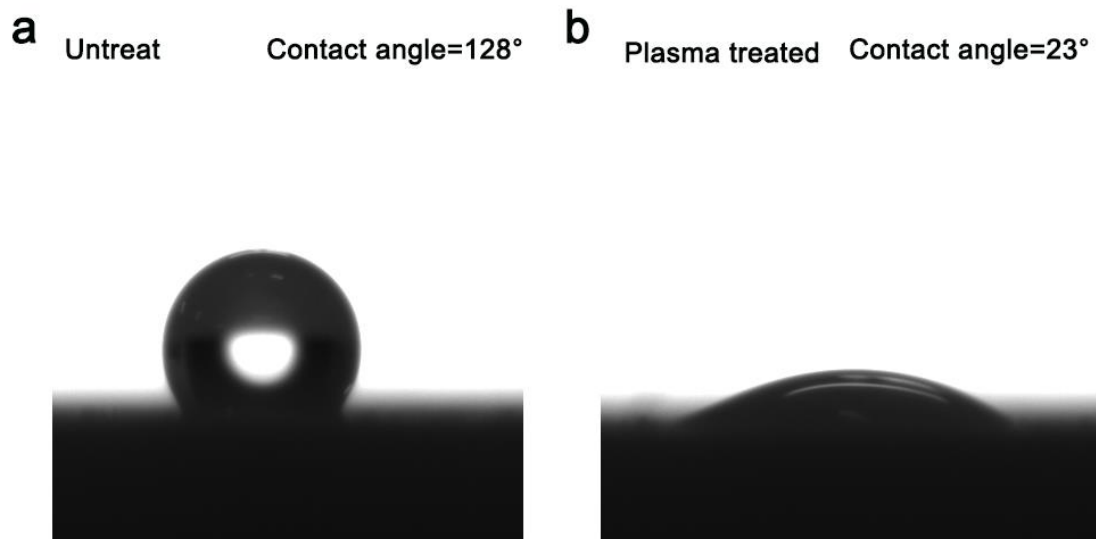


Fig.S8 Water contact angle of GO-Doped PU nanofibrous membrane before (a) and after (b) low-temperature oxygen plasma treatment.

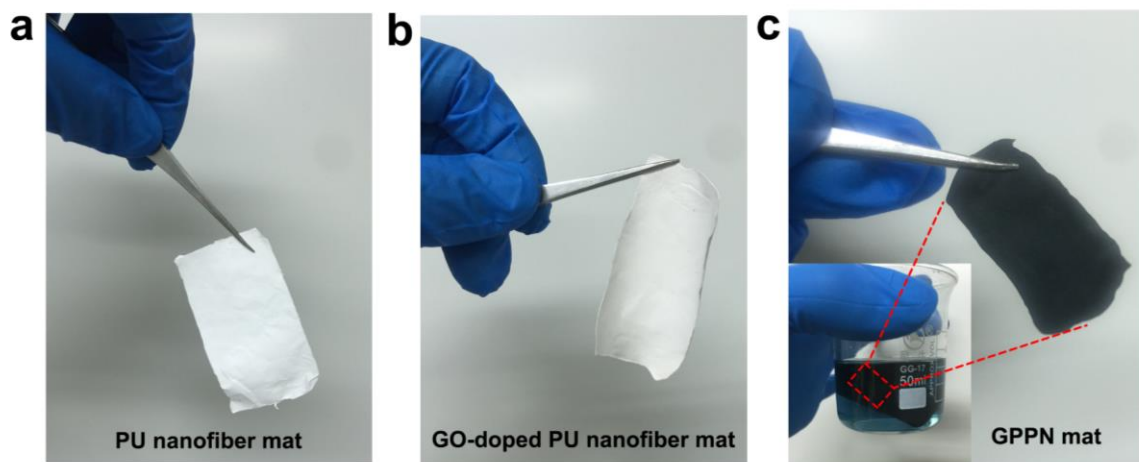


Fig.S9 (a) Photograph of an electrospun PU nanofiber mat, (b) photograph of an electrospun GO-doped PU nanofiber mat, and (c) photograph of a GPPN mat made from (b).

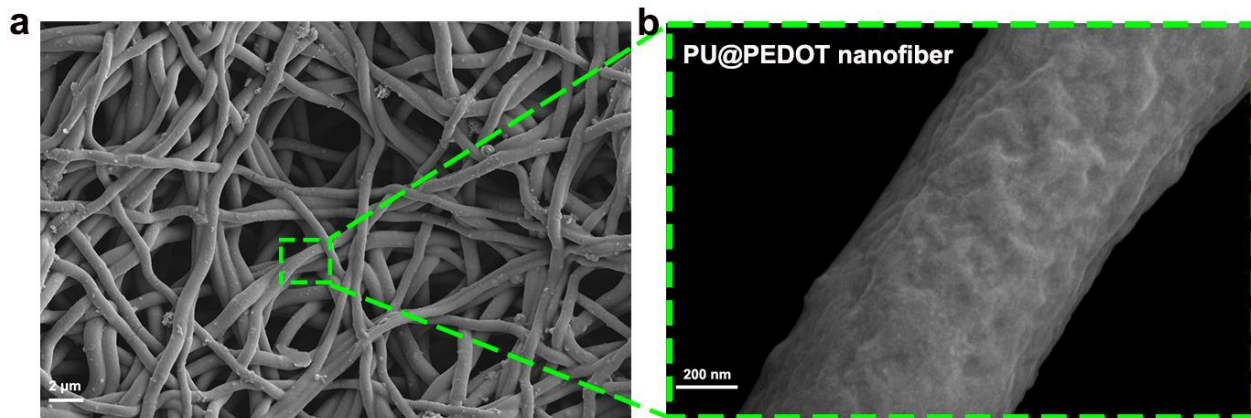


Fig.S10 (a) Low-and (b) high-magnification SEM images of the PU@PEDOT nanofibrous membrane.

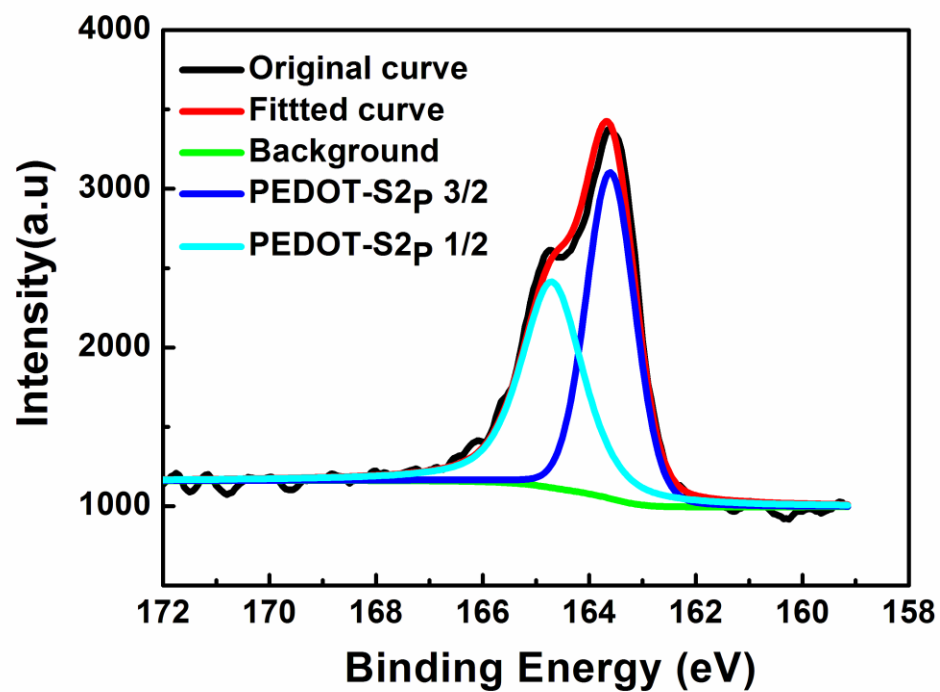


Fig. S11 XPS results of the S_{2p} spectrum of PEDOT in the GPPN membrane.

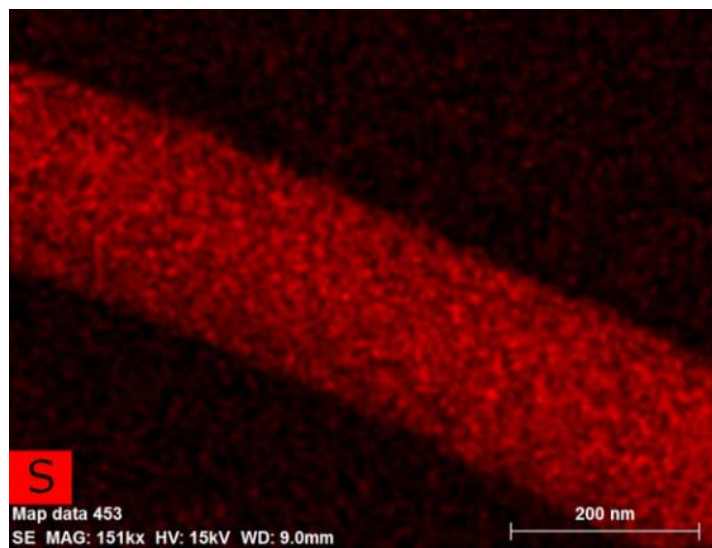


Fig. S12 EDS mapping images of a GPPN.

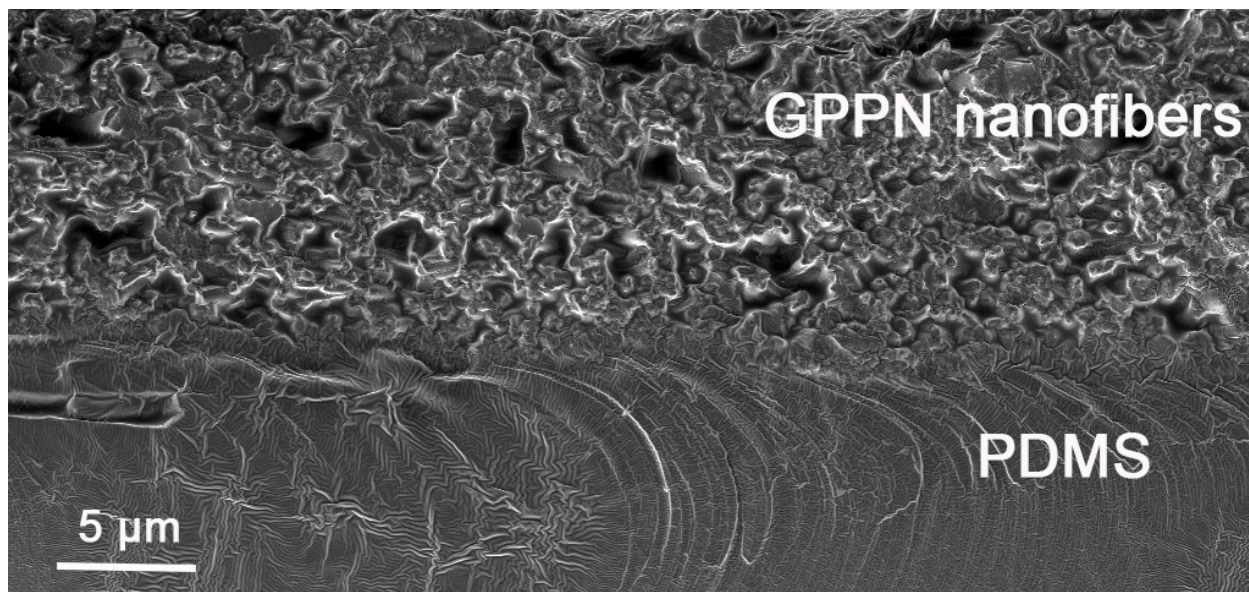


Fig. S13 The cross-SEM of PDMS-coated GPPN sensor. The van der Waals contribute to the firm bonding of PDMS layer with GPPN membrane.

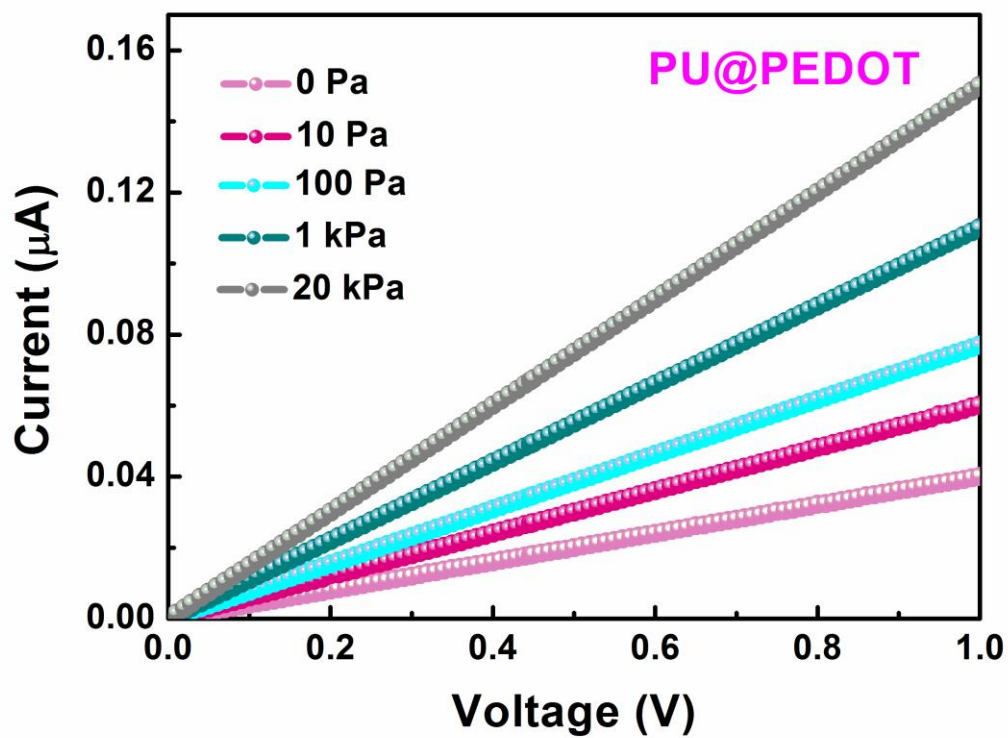


Fig. S14 I-V curves of the PU@PEDOT nanofiber (PPN) sensor under different pressure loading conditions (0-20 kPa).

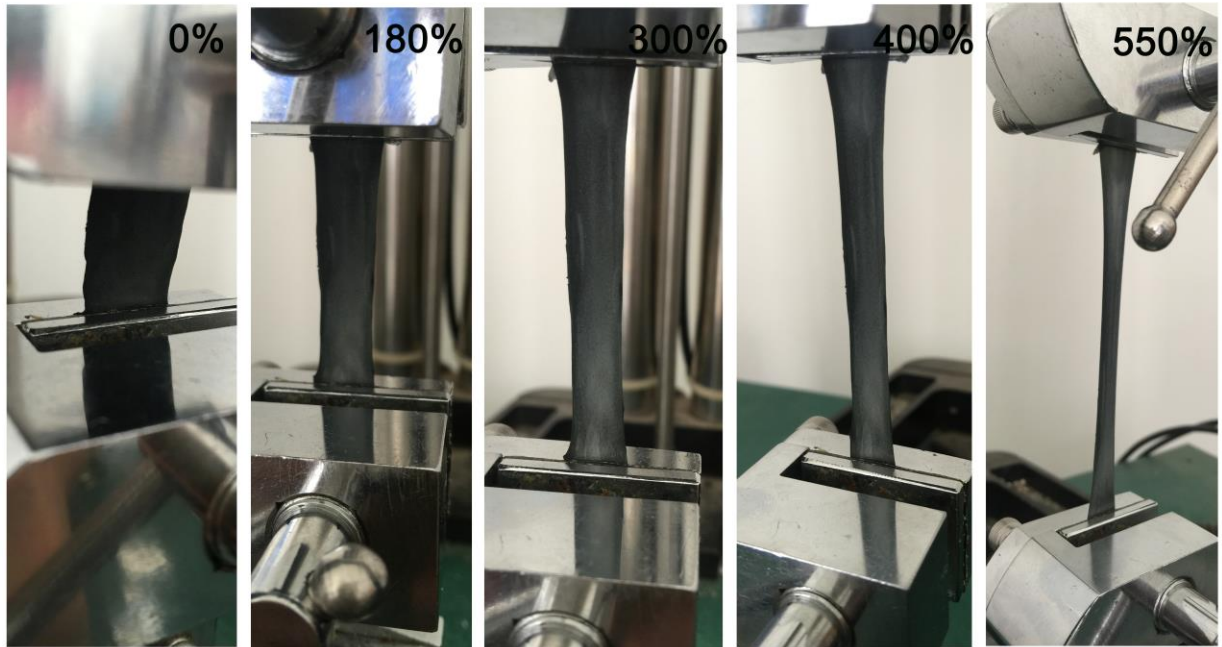


Fig. S15 Photographs of a GPPN sensor during loading of increasing strain.

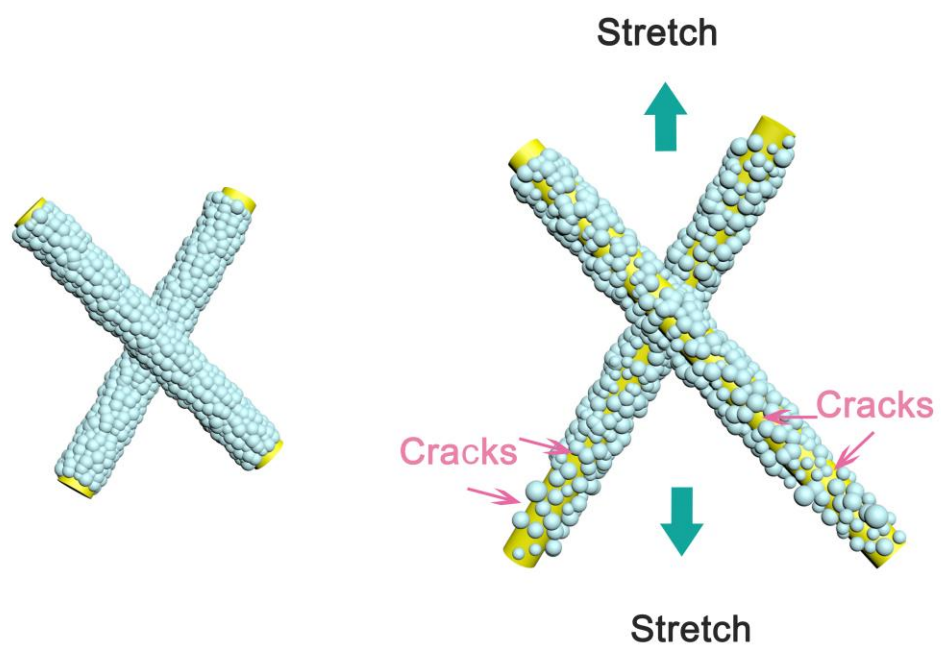


Fig. S16 The sensing mechanism of the stretchable GPPN sensor.

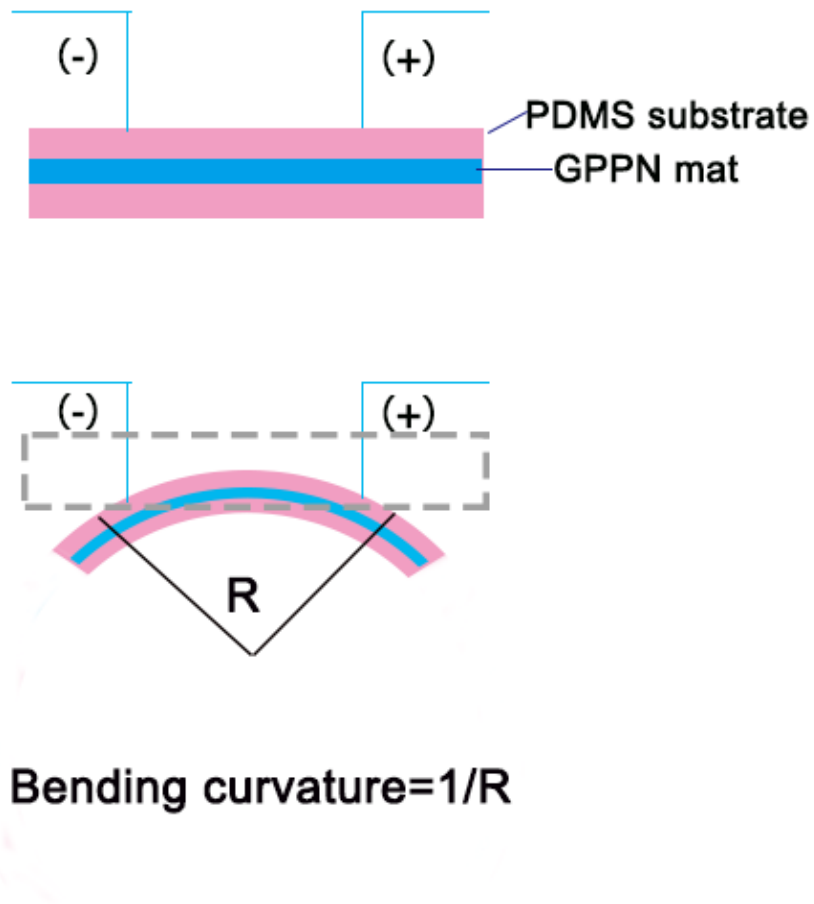


Fig.S17 Schematic illustration of the test methods for the bending mechanical stimuli.

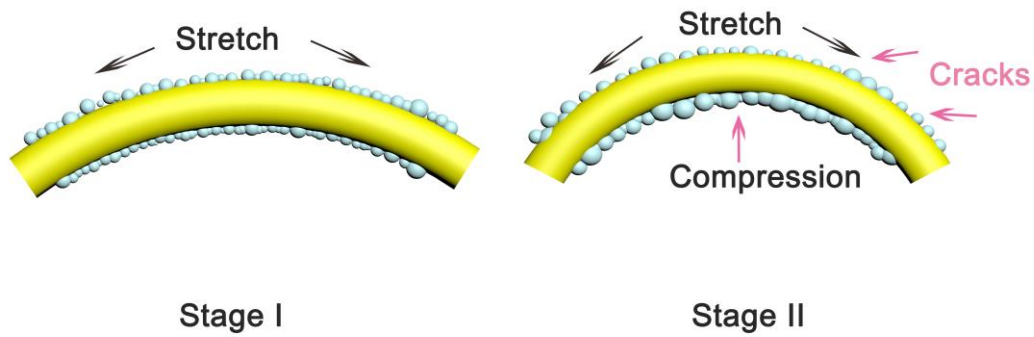


Fig.S18 Schematic illustration of the bending sensing mechanism.

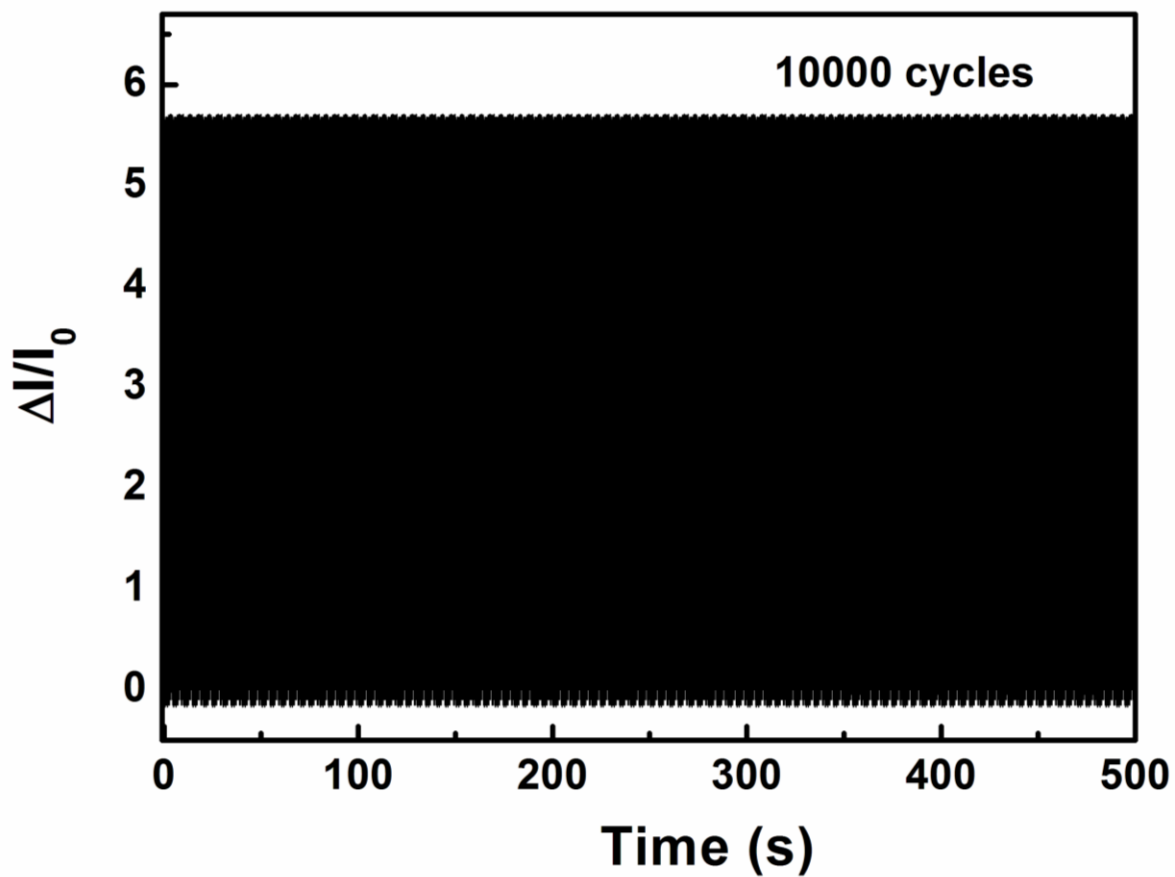


Fig.S19 Performance of the GPPN sensor during 100,000 loading-unloading cycles under an applied pressure of 500 Pa, showing stability and durability.

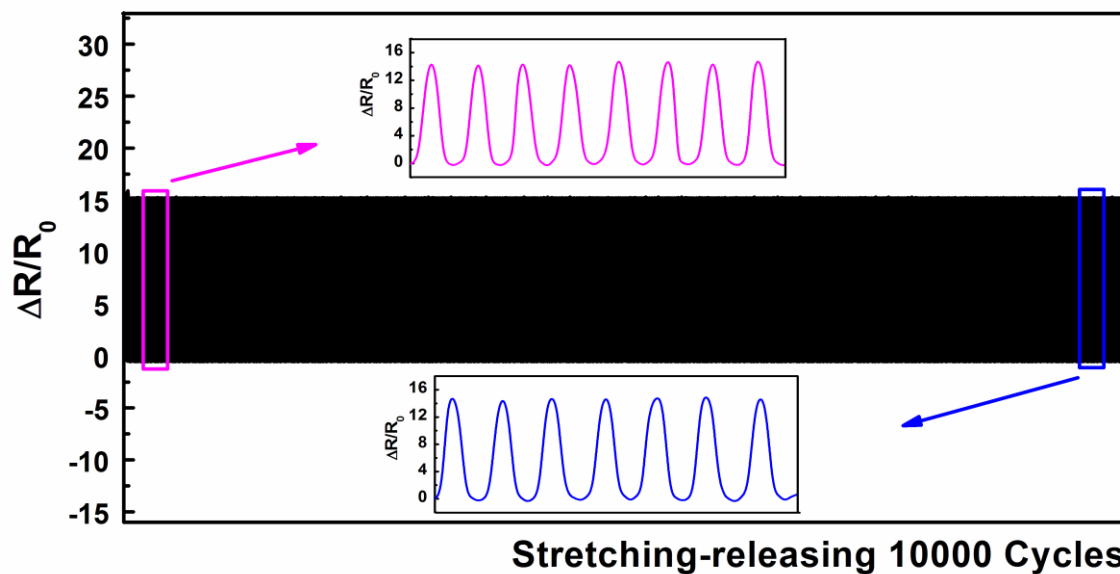


Fig.S20 Performance of the GPPN sensor during 10,000 stretching-releasing cycles of a larger strain of 120%, indicating its remarkable stability and durability.

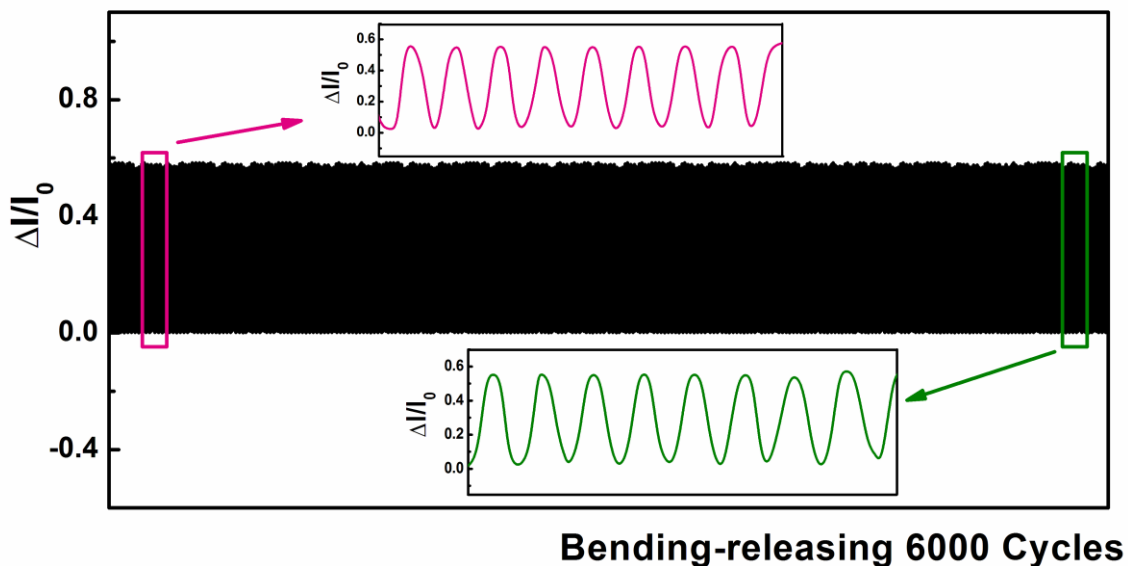


Fig.S21 Performance of the GPPN sensor during 6000 bending-releasing cycles under a bending curvature of 0.6 cm^{-1} , showing stability and durability.

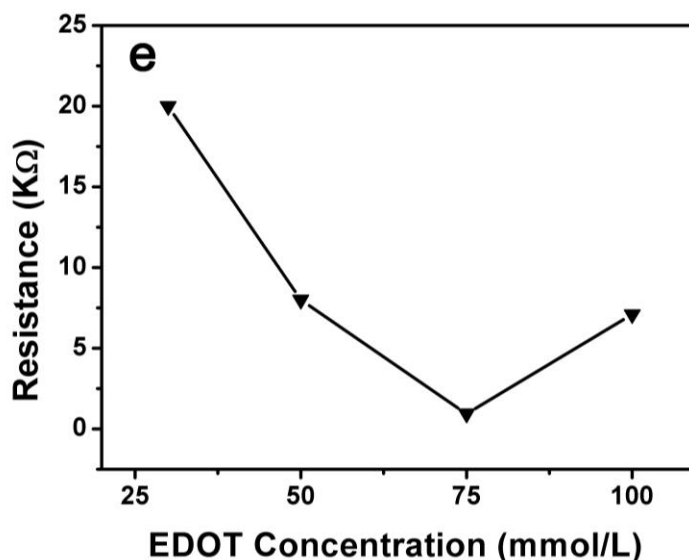
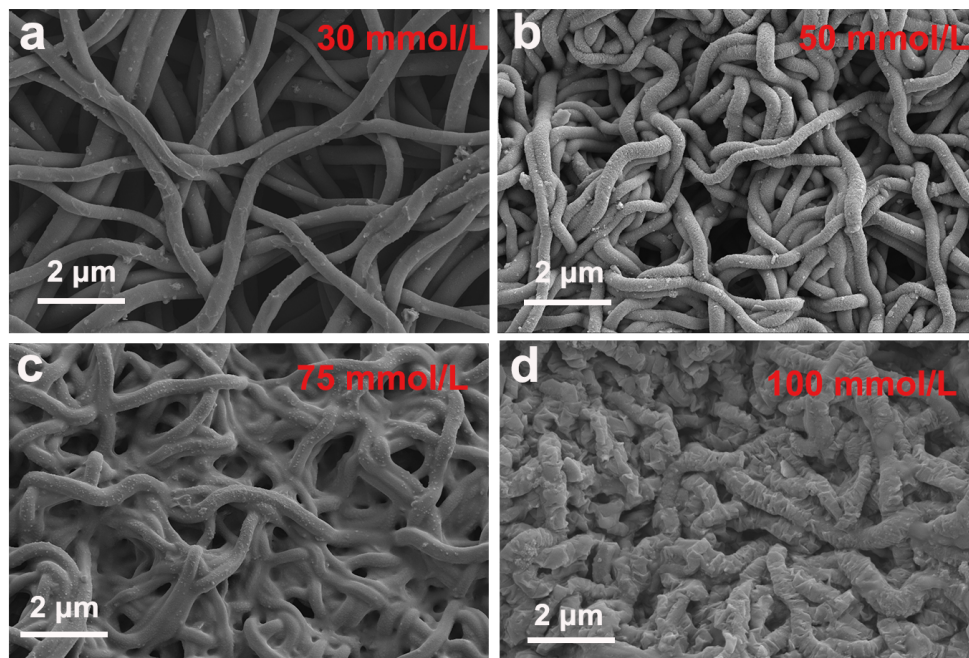


Fig. S22 The SEM images of the GPPN membranes prepared with different concentration of EDOT solution(a-d). (e) Curves of resistance of GPPN membranes against EDOT concentration. The thickness of the PEDOT layer increased with the with the increase of EDOT monomer concentration. Significant drop in electrical resistance can be observed firstly with the increase of EDOT monomer concentration (< 75 mmol/L), While, with further increase of EDOT monomer concentration, the electrical resistance trends to become increase. When the concentration is lower, the number of EDOT molecules per unit volume increases gradually with the increase of monomer concentration, which in favour of the oxidation and polymerization of EDOT. Whereas the speed of polymerization is too fast with higher concentration, resulting in unevenly coating on the surface of nanofiber mats of the generated PEDOT nanoparticles. Instead, the electrical resistance increase.

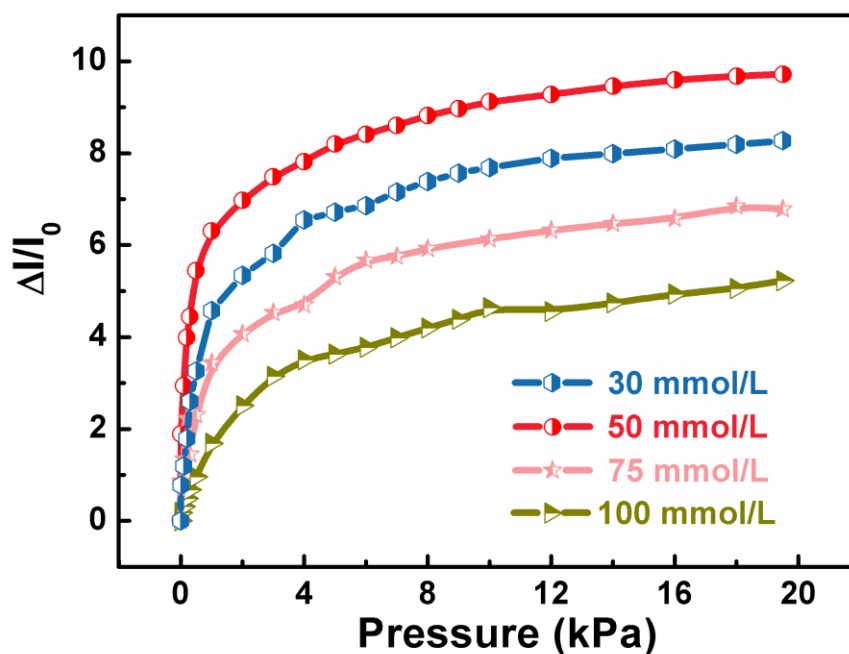


Fig. S23 Comparison of the pressure sensitivity of the GPPN sensor with different EDOT concentration. The sensitivity of the GPPN sensor increases firstly, with the increase of EDOT monomer concentration from 30 mmol/L to 50 mmol/L. As seen in Fig. S22b, the nanofibers with a continuous-coating PEDOT nanoparticulates layer could provide more contact sites and more conductive networks, thus facilitating electron transfer and giving a higher pressure sensitivity when subjected to the same applied pressure. While the pressure sensitivity trends to become decrease with further increase of EDOT monomer concentration. This is due to that the conductive nanofibers with dense and thick PEDOT layer need larger applied pressure to produce deformation and increase of the contact area.

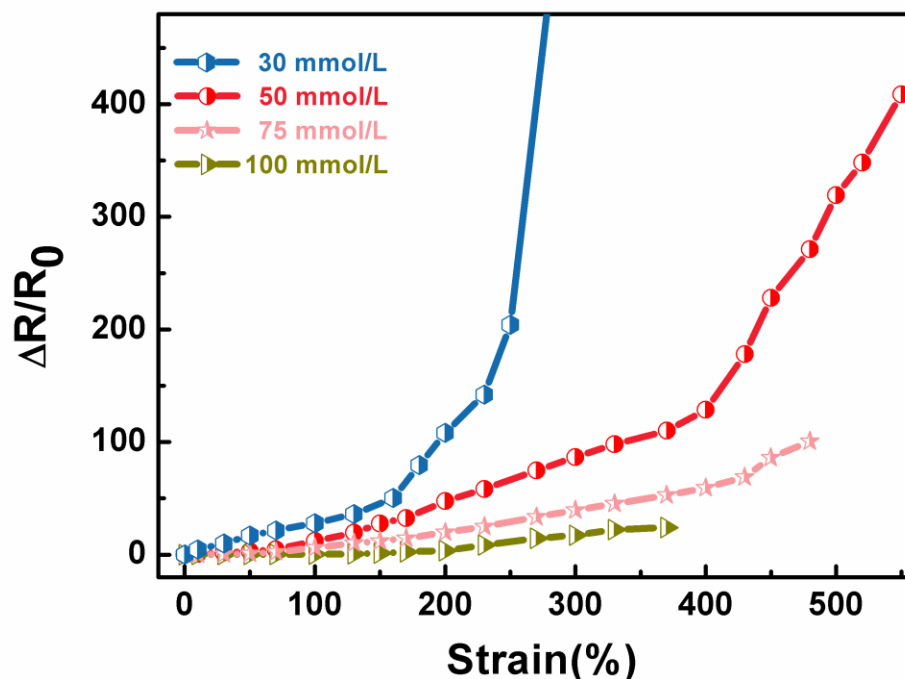


Fig. S24 Comparison of the strain sensitivity of the GPPN sensor prepared with different EDOT concentration. The GPPN sensor with thinner thickness of the PEDOT layer exhibits higher sensitivity to external strain. Because that their conductive networks are brittle and the micro-cracks easy to be opened. Therefore, the resistance of the GPPN sensor is increased by the opening of micro-cracks between PEDOT nanoparticles during the elongation process. during the stretching. On the contrary, the GPPN sensors with a higher EDOT concentration exhibit lower sensitivity to strain stimuli. This is due to that the opening of micro-cracks during the stretching process is difficult under small strain. In addition, the GPPN sensors prepared with higher EDOT concentration have relative poor flexibility and stretchability.

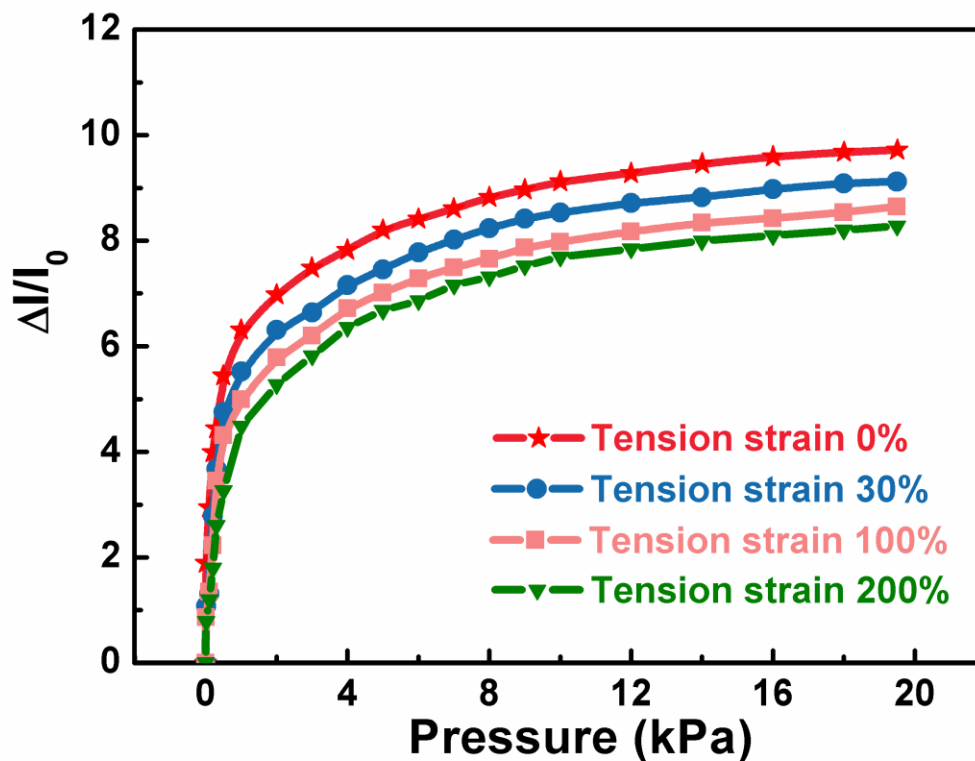


Fig.S25 The plots of the current change of the GPPN sensor under various tensile strain as a function of the applied pressure. It can be seen that the sensitivities at stage I decrease to 88.4%, 73.4%, 59.3%, at 30%, 100%, and 200% of tensile strain, respectively, and the sensitivities at stage II and stage III almost keep the same value as that of the original value. Therefore the sensor can be applied on arbitrary curved and moving surface and keep more than 50% of its original pressure sensitivity.

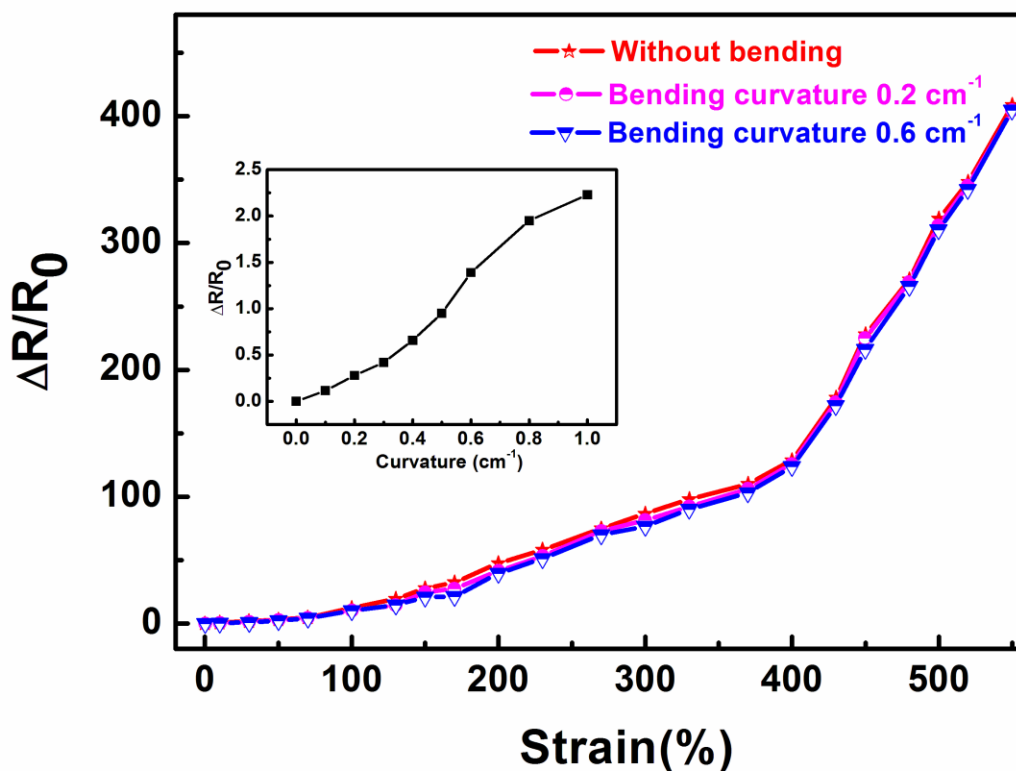


Fig.S26 The plots of the resistance change of the GPPN sensor under various bending curvature as a function of the tensile strain. The inset shows the relative resistance variation of GPPN sensor upon bending to different curvature. To study the GF of the sensor under the bending state, the relative resistance change versus applied tensile strain of the sensor under different bending state were performed and shown in the Figure S26. It can be seen that the sensitivities at 0.2 cm^{-1} , and 0.6 cm^{-1} of bending curvature almost keep the same value as that of the original value. As shown in the inset of the Figure. S26, the relative resistance changes under the bending state are small enough and thus hardly disturbs the precise tensile strain sensing. Such properties make the GPPN sensor suitable to be mounted on arbitrary curved and moving surface, exhibiting superior performance under some special conditions.

Table. 1 Performance criteria comparison of nanofiber-based flexible sensor

Nanofiber-based sensor	Sensitivity (Pressure)	Sensing range	Stretchability	Gauge factor	Reference
Carbonized silk nanofiber membrane	34.47 kPa ⁻¹	0.8-5000 Pa	-	-	[S1]
Reversible interlocking of nanofibres	11.45	5-1500 Pa	-	-	[S2]
Interlocking elastic patterned nanofibrous membranes.	1.24 kPa ⁻¹	1.3-7000 Pa	-	-	[S3]
RGO-encapsulated P(VDF-TrFe) nanofibers	15.6 kPa ⁻¹	1.2-55000 Pa	-	-	[S4]
Gold nanowire-impregnated tissue paper	1.14 kPa ⁻¹	50000 Pa	25%	7.38 below 14% 1.82 (14%-25%)	[S5]
Graphene/free-standing nanofibrillar PEDOT/P(VDF-HFP) hybrid	-	0.5 to 30 Pa	2%	320 (0.2% strain)	[S6]
Electrospun carbon nanofibers	-	-	300%	72 (300%)	[S7]
Carbon nanotube fiber on pre-strain Ecoflex	-	-	960%	0.56 (200%); 47 (200%-400%); 64 (400-960%)	[S8]
Nanofibrous PANI/PVDF based onelectrospinning and in-situ polymerization			110%	0.045 (<85%) 0.84 (85% to 110%)	[S9]
3D elastic porous GO-doped PU@PEDOT nanofiber membrane	20.6 kPa⁻¹	1-20000 Pa	550%	10.1 (<100%); 34.8 (100%-400%); 193.2 (400-550%)	This work

References for Supporting Information:

- [S1] Wang, Q.; Jian, M.; Wang, C.; & Zhang, Y. Carbonized Silk Nanofiber Membrane for Transparent and Sensitive Electronic Skin. *Adv. Funct. Mater.* **2017**, *27*(9), 1605657.
- [S2] Pang, C.; Lee, G. Y.; Kim, T. I.; Kim, S. M.; Kim, H. N., & Ahn, S. H., et al. A Flexible and Highly Sensitive Strain-Gauge Sensor Using Reversible Interlocking of Nanofibres. *Nat Mater.* **2012**, *11*(9), 795-801.
- [S3] Zhong, W.; Liu, Q.; Wu, Y.; Wang, Y.; Qing, X., & Li, M., et al. A Nanofiber Based Artificial Electronic Skin with High Pressure Sensitivity and 3d Conformability. *Nanoscale.* **2016**, *8*(24), 12105.
- [S4] Lou, Z.; Chen, S.; Wang, L.; Jiang, K., & Shen, G. An Ultra-Sensitive and Rapid Response Speed Graphene Pressure Sensors for Electronic Skin and Health Monitoring. *Nano Energy.* **2016**, *23*, 7-14.
- [S5] Gong, S.; Schwalb, W.; Wang, Y.; Chen, Y.; Tang, Y., & Si, J., et al. A Wearable and Highly Sensitive Pressure Sensor with Ultrathin Gold Nanowires. *Nat. Commun.* **2014**, *5*(2), 3132.
- [S6] Jin, W. P., & Jang, J. Fabrication of Graphene/Free-Standing Nanofibrillar Hybrid PEDOT/P(VDF-HFP) Device for Wearable and Sensitive Electronic Skin Application. *Carbon*, **2015**, *87*, 275-281.
- [S7] Ding, Y.; Yang, J.; Tolle, C. R., & Zhu, Z. A Highly Stretchable Strain Sensor Based on Electrospun Carbon Nanofibers for Human Motion Monitoring. *RSC Adv.* **2016**, *6*(82), 79114-79120.
- [S8] Ryu, S.; Lee, P.; Chou, J. B.; Xu, R.; Zhao, R., & Hart, A. J., et al. Extremely Elastic Wearable Carbon Nanotube Fiber Strain Sensor For Monitoring of Human Motion. *ACS Nano.* **2015**, 5929. B
- [S9] Yu, G. F.; Yan, X.; Yu, M.; Jia, M. Y.; Pan, W.; He, X. X. Patterned, Highly Stretchable and Conductive Nanofibrous PANI/PVDF Strain Sensors Based on Electrospinning and in situ Polymerization. *Nanoscale*, **2016**, *8*(5), 2944-2950.